Effects of Zn, Cu, and K promoters on the structure and on the reduction, carburization, and catalytic behavior of iron-based Fischer–Tropsch synthesis catalysts

Senzi Li, Anwu Li, Sundaram Krishnamoorthy and Enrique Iglesia *

Department of Chemical Engineering, University of California, Berkeley, CA 94720, USA
E-mail: iglesia@cchem.berkeley.edu

Zn, K, and Cu effects on the structure and surface area and on the reduction, carburization, and catalytic behavior of Fe–Zn and Fe oxides used as precursors to Fischer–Tropsch synthesis (FTS) catalysts, were examined using X-ray diffraction, kinetic studies of their reactions with H_2 or CO, and FTS reaction rate measurements. Fe_2O_3 precursors initially reduce to Fe_3O_4 and then to metallic Fe (in H_2) or to a mixture of $Fe_{2.5}C$ and Fe_3C (in CO). Zn, present as $ZnFe_2O_4$, increases the surface area of precipitated oxide precursors by inhibiting sintering during thermal treatment and during activation in H_2/CO reactant mixtures, leading to higher FTS rates than on ZnO-free precursors. $ZnFe_2O_4$ species do not reduce to active FTS structures, but lead instead to the loss of active components; as a result, maximum FTS rates are achieved at intermediate Zn/Fe atomic ratios. Cu increases the rate of Fe_2O_3 reduction to Fe_3O_4 by providing H_2 dissociation sites. Potassium increases CO activation rates and increases the rate of carburization of Fe_3O_4. In this manner, Cu and K promote the nucleation of oxygen-deficient FeO_x species involved as intermediate inorganic structures in reduction and carburization of Fe_2O_3 and decrease the ultimate size of the Fe oxide and carbide structures formed during activation in synthesis gas. As a result, Cu and K increase FTS rates on catalysts formed from Fe–Zn oxide precursors. Cu increases CH_4 and the paraffin content in FTS products, but the additional presence of K inhibits these effects. Potassium titrates residual acid and hydrogenation sites and increases the olefin content and molecular weight of FTS products. K increases the rate of secondary water–gas shift reactions, while Cu increases the relative rate of oxygen removal as CO_2 instead of water after CO is dissociated in FTS elementary steps. Through these two different mechanisms, K and Cu both increase CO_2 selectivities during FTS reactions on catalysts based on Fe–Zn oxide precursors.

KEY WORDS: Fischer–Tropsch synthesis; promoters; iron; carbide; copper; potassium; zinc

1. Introduction

Iron oxides act as precursors for Fischer–Tropsch synthesis (FTS) catalysts, which convert synthesis gas (H_2/CO) to useful chemicals and liquid hydrocarbons [1–4]. These oxides transform into active structures during initial contact with synthesis gas at typical reaction temperatures. Several Fe phases, such as Fe metal, Fe carbides (FeC_x) or oxides (FeO_x) form; most of them have been proposed at some point to act as active structures during steady-state Fischer–Tropsch synthesis [5–12]. Oxides (ZnO, MnO, Al_2O_3), metals (Cu, Ru), and alkali (K, Na, Cs, Rb) oxides or carbonates are typically added to Fe oxide precursors as promoters in order to improve their structural integrity or catalytic properties. For example, ZnO, Cu, and K compounds have been reported to increase FTS rates on precipitated Fe_2O_3 precursors [13–17]. Earlier studies suggested that K promotes CO chemisorption and inhibits H_2 chemisorption, which in turn leads to lower FTS rates, higher product molecular weight, and greater olefin content [3,14], although it is unclear how the prevalent K_2CO_3 and FeC_x species interact in order to produce the atomic contact required for the proposed electronic effects. Cu, when present along with K, increases FTS

rates without detectable changes in selectivity [17,18]. Cu and K compounds have been reported to increase the activity for water–gas shift (WGS) [14,16], a reaction that occurs concurrently with FTS on many Fe-based catalysts. Our previous studies have shown that Cu or Ru oxides in intimate mixtures with a Fe–Zn–K precursor matrix increase the rate of reduction and carburization of the Fe oxide component in these precursors, and leads to the formation of smaller FeC_x crystallites, to greater active site densities, and to higher FTS rates [17,19,20]. Hence, Cu and Ru do not act as chemical promoters, but instead provide a better dispersion of the active phase and a greater availability of active sites.

We examine here co-precipitated Fe and Zn oxides containing Zn, Cu and K (Zn/Fe = 0–0.4, K/Fe = 0–0.04, and Cu/Fe = 0–0.02 atomic ratios) in order to probe the roles of each component on the structure and on the reduction, carburization, and catalytic behavior of Fe oxides. The surface area, bulk structure, and reduction and carburization kinetics were systematically investigated using BET surface area measurements, X-ray diffraction (XRD) and temperature-programmed reaction (TPR) studies. In parallel, steady-state FTS rates and selectivities were measured as a function of the Zn, K, and Cu contents at realistic FTS conditions (493 K, 3.16 MPa) using a tubular reactor with plug-flow hydrodynamics in order to relate the observed catalytic pro-

---

* To whom correspondence should be addressed.

motion to the active structures formed during activation of Fe–Zn oxide precursors in H_2/CO mixtures.

2. Experimental

2.1. Synthesis of Fe_2O_3–Zn–K–Cu catalysts

Fe_2O_3–Zn–K–Cu catalysts were prepared by co-precipitation of Fe and Zn nitrates at a constant pH to form porous Fe–Zn oxyhydroxide powders, which were promoted by impregnation with K_2CO_3 and $Cu(NO_3)_2$ after treatment in air. A solution containing both $Fe(NO_3)_3$ (Aldrich, 99.9+%, 3.0 M) and $Zn(NO_3)_2$ (Aldrich, 99.9+%, 1.4 M) with varying atomic ratios (0–0.4) and a separate solution of $(NH_4)_2CO_3$ (Aldrich, 99.9%, 1 M) were used in the precipitation process. The Zn/Fe solution was added (120 cm^3/h) into a flask containing deionized water ($\sim$50 cm^3) at 353 K using a liquid pump. $(NH_4)_2CO_3$ was added simultaneously and its rate was controlled in order to keep the pH of the slurry at 7.0 ± 0.1 (Omega, PHB-62 pH meter). The precipitated powders ($\sim$20 g) were washed five times with doubly distilled deionized water ($\sim$1000 cm^3/g each time), and dried in ambient air at 393 K overnight. The dried precursors were then treated in flowing dry air at 623 K for 1 h.

Promoters were added to these precursors by impregnation with aqueous solutions of K_2CO_3 (Aldrich, 99.99%, 0.16 M) and/or $Cu(NO_3)_2$ (Aldrich, 99.99%, 0.16 M) to give the desired K/Fe and Cu/Fe atomic ratios. The impregnated samples were dried at 393 K in ambient air and then treated in flowing dry air at 673 K for 4 h, a procedure that led to the complete decomposition of all precursor salts except K_2CO_3 [21]. The resulting powders consisted of CuO, ZnO, Fe_2O_3, and K_2CO_3, as shown by chemical analysis, identification of decomposition products, X-ray diffraction, and X-ray absorption spectroscopy.

These samples are denoted as Fe_2O_3–Zn–Cu_x, Fe_2O_3–Zn–K_y, or Fe_2O_3–Zn–K_y–Cu_x, where x and y represent the atomic ratios of the respective elements relative to Fe. All samples were pressed into pellets (443 MPa), crushed, and sieved to retain 100–180 μm particles.

2.2. Catalyst characterization

Powder X-ray diffraction (XRD) measurements were carried out using a D-5000 Siemens diffractometer and Cu Kα radiation ($\lambda = 1.5406$ Å). BET surface areas were measured using an Autosorb 6 automated system (Quantachrome, Inc.) and N_2 physisorption at its normal boiling point, after evacuating the samples at 393 K for 3 h.

The rates of reduction and carburization of K- and/or Cu-promoted Fe_2O_3–Zn were measured by using temperature-programmed reaction (TPR) methods and H_2 (Airgas, 99.999%) or CO (Matheson, 99.999%) as reactants. Samples (0.2 g) were placed in a quartz cell (10 mm i.d.) and first treated in 20% O_2 in Ar (Airgas, 99.99%, 0.268 mol/h) by heating to 673 K at 0.33 K/s, holding at 673 K for 900 s,

and then cooling to ambient temperature in Ar. The flow was then switched to 20% H_2 or 20% CO in Ar (0.268 mol/h) and the reactor temperature was increased to 1000 K at 0.167 K/s. The concentration of reactants and products was measured using a mass spectrometer (Leybold Inficon Instruments Co., Inc.) equipped with a differentially pumped sampling system.

2.3. Fischer–Tropsch synthesis rates and selectivities

Steady-state FTS reaction rates and selectivities were measured in a single-pass fixed-bed reactor (SS 304, 1.27 cm o.d. and 1 cm i.d.) held within by a three-zone furnace equipped with temperature controllers (Watlow series 982 and 988). The bed temperature was monitored axially using a type-K movable thermocouple; it was within ± 0.5 K of the average bed temperature throughout the reactor length. All lines after the reactor outlet were kept at 433–553 K. The reactor system also included two stainless steel 75 cm^3 traps. A heated trap (at 408 K and reactor pressure) was placed immediately below the reactor in order to collect heavy hydrocarbons and a cold trap (at ambient temperature and pressure) was placed after the gas chromatograph sampling valve in order to collect water, oxygenates, and C_{15-} hydrocarbons.

Synthesis gas (Praxair, 62% H_2, 31% CO and 7% N_2, N_2 internal standard) was purified by removing metal carbonyls (activated charcoal trap, Sorb-Tech RL-13) and water (molecular sieve trap, Matheson, model 452A). Synthesis gas flow rates were controlled using an electronic mass-flow controller (Porter, model 201-AFASVCAA). Catalyst samples (0.4 g, 100–180 μm) diluted with quartz granules (11 g, 100–180 μm) were activated in synthesis gas at 0.1 MPa by increasing the temperature from 298 to 423 K at 0.167 K/s and then from 423 to 543 K at 0.017 K/s. The samples were kept at 543 K for 1 h, before setting the reaction temperature and pressure (493 K and 3.16 MPa). Product and reactant analysis was carried out by gas chromatography (Hewlett–Packard, model 5890 series II) using a ten-port sampling valve. The analysis of N_2, CO, CO_2, and light hydrocarbons was performed using a thermal conductivity detector and a Porapak Q packed column (15.2 cm $\times$ 0.318 cm). All hydrocarbons up to C_{15} were analyzed using a flame ionization detector and a cross-linked methyl silicone capillary column (HP-1, 50 m $\times$ 0.32 mm; 1.05 μm film).

3. Results and discussion

3.1. Crystalline structures in Fe_2O_3–Zn precursors

X-ray powder diffraction patterns for Fe_2O_3–Zn precursors with Zn/Fe atomic ratios of 0–0.4 are shown in figure 1. These diffraction data indicate that rhombohedral hematite (Fe_2O_3), with a corundum-type structure, forms in samples with Zn/Fe < 0.2, while a $ZnFe_2O_4$ phase with a cubic

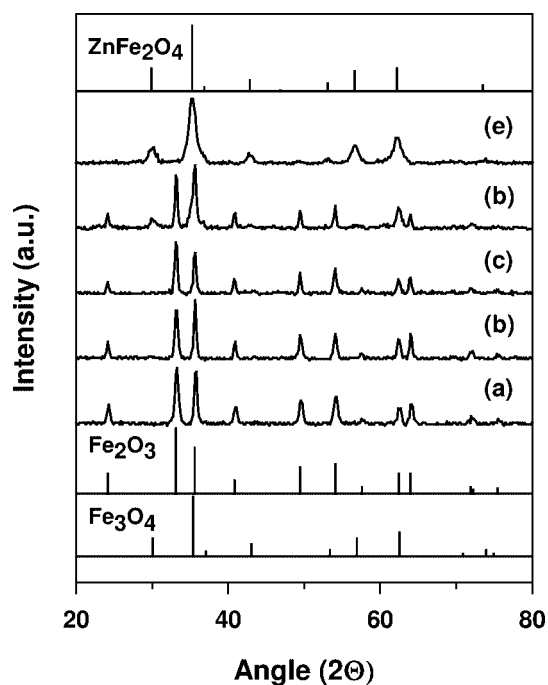Figure 1. X-ray diffraction patterns of Fe_2O_3–Zn samples with different Zn/Fe ratios: (a) 0, (b) 0.05, (c) 0.1, (d) 0.2, and (e) 0.4.

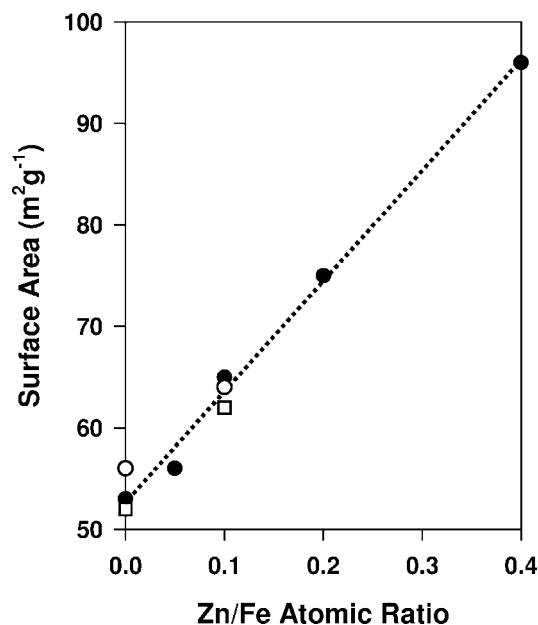Figure 2. BET surface areas of K- and/or Cu-promoted Fe_2O_3–Zn (K/Fe = 0.02, Cu/Fe = 0.01) samples as a function of Zn/Fe ratios: (●) Fe_2O_3–Zn–K_2–Cu_1 sample, (○) Fe_2O_3–Zn–Cu_1 sample, and (□) Fe_2O_3–Zn–K_2 sample.

franklinite spinel-type structure appears along with hematite at higher Zn/Fe ratios. Fe_2O_3 and $ZnFe_2O_4$ co-exist at intermediate Fe/Zn ratios. $ZnFe_2O_4$ is the only detectable phase in the sample with the highest Zn/Fe ratio (0.4); its broad diffraction peaks reflect the Zn-deficient nature of the Fe–Zn spinel structure, which requires a Zn/Fe ratio of 0.5 for stoichiometric $ZnFe_2O_4$. Precipitated Fe–Zn oxides appear to be present in the form of a mixture of Fe_2O_3 and $ZnFe_2O_4$. The only Zn-containing phase is $ZnFe_2O_4$, and it acts as a textural promoter that increases the surface area of Fe_2O_3–Zn precursors, as shown in section 3.2. At low Zn concentrations (figure 1, patterns (a)–(c)), Zn is detected only as small $ZnFe_2O_4$ crystallites, which appear to inhibit the sintering of Fe_2O_3 at high temperatures (623–673 K). At higher Zn contents (figure 1, patterns (d) and (e)), it is likely that $ZnFe_2O_4$ crystallites provide a matrix for the isolation of Fe_2O_3 crystallites. Zn consumes some of the Fe oxide precursors, however, in forming $ZnFe_2O_4$, a less reducible compound than Fe_2O_3; this tends to weaken the structural promotion by Zn by preventing the reduction of some of the Fe and its contribution to the formation of FTS active sites. Thus, intermediate Zn/Fe ratios are likely to lead to optimum catalytic performance. The impregnation of potassium and copper and the subsequent treatment of these samples in air did not influence the Fe–Zn oxide crystalline phases detected by X-ray diffraction. This shows that Fe–Zn oxide structures, once formed, remain stable during subsequent aqueous impregnation and thermal treatment.

3.2. Surface areas of Fe_2O_3–Zn–K–Cu oxide precursors

The textural promotion effects of $ZnFe_2O_4$ on the surface area of Fe oxide precursors were examined by N_2 physisorp-

tion measurements Fe_2O_3–Zn promoted with K and/or Cu. Fe_2O_3–Zn–K–Cu surface areas increased monotonically with increasing Zn/Fe ratio (figure 2). The surface area for the sample with a Zn/Fe ratio of 0.4 was almost twice that for Zn-free Fe_2O_3 (96 vs. 53 m^2/g). The addition of K and/or Cu to Fe–Zn oxides did not influence surface areas, suggesting that K and Cu reside at Fe oxide crystallite surfaces and that they do not influence the structure or dispersion of Fe oxide phases. These data suggest that Zn as a $ZnFe_2O_4$ phase inhibits the sintering of Fe oxides, by keeping Fe oxides from sintering during thermal treatments or by providing anchoring or nucleation sites for Fe oxides during precipitation or thermal treatment. It is unclear, however, whether this textural promotion by Zn alone can account for the higher FTS rates observed on Zn-promoted samples [14] or what Zn/Fe ratios lead to maximum rates. Therefore, we examine next the catalytic properties of K- and Cu-promoted Fe oxides with varying Zn/Fe ratios.

3.3. Zn promotion effects on Fischer–Tropsch synthesis rates and selectivity

Steady-state FTS rates and selectivities (493 K, 3.16 MPa) on Fe_2O_3–Zn–K–Cu catalysts with a constant K and Cu content (K/Fe = 0.02, Cu/Fe = 0.01) but different Zn contents are shown in table 1 at similar CO conversion levels. The presence of Zn at a Zn/Fe atomic ratio of 0.1 leads to higher CO conversion rates than on a Zn-free catalyst (2.4 vs. 1.5 mol-CO/h g-at.-Fe), but higher Zn/Fe ratios (0.1–0.4) did not further increase FTS rates. The higher surface areas of these Zn-rich samples occur at the expense of reactions of ZnO with Fe oxide precursors to form unreducible $ZnFe_2O_4$. FTS selectivities (CH_4, C_{5+}, and 1-pentene/n-

Table 1

Effect of Zn loading on the surface area and the steady state performance of a Fe_2O_3–K–Cu catalyst (K/Fe = 0.02, Cu/Fe = 0.01; H_2/CO = 2, 493 K, 3.16 MPa, CO conversion 16–18%).

Sample	Zn/Fe		
	0	0.1	0.4
Surface area (m^2/g)	53	65	96
CO conversion rate (mol-CO/h g-at.-Fe)	1.52	2.40	2.63
CO_2 formation rate (mol-CO/h g-at.-Fe)	0.19	0.30	0.21
Hydrocarbon formation rate (mol-CO/h g-at.-Fe)	1.33	2.10	2.52
CO_2 selectivity (%)	12.3	12.3	7.6
CH_4 selectivity (%)[a]	1.7	1.8	2.3
C_{5+} selectivity (%)[a]	86.6	87.6	85.6
1-C_5H_{10}/n-C_5H_{12} ratio	1.9	1.8	2.0

[a] CH_4 and C_{5+} selectivities are reported on a CO_2-free basis.

Figure 3. Oxygen removal rates of Fe_2O_3–Zn–K–Cu (Zn/Fe = 0.1) in H_2: (a) CuO, (b) Fe_2O_3–Zn (c) Fe_2O_3–Zn–Cu_1, (d) Fe_2O_3–Zn–K_2, and (e) Fe_2O_3–Zn–K_2–Cu_1 (0.2 g sample, 0.167 K/s ramping rate, 20% H_2/Ar, 0.268 mol/h flow rate).

pentane ratios) were almost unchanged by the presence of Zn. It appears that Zn acts only as a textural promoter and that a Zn/Fe atomic ratio of ∼0.1 provides an optimum balance between its textural promotion effects and its tendency to react with Fe oxide precursors and prevent their activation during FTS. Therefore, a Zn/Fe atomic ratio of 0.1 was chosen to study the effects of Cu and K on FTS reaction rates and selectivities.

3.4. Reduction kinetics of Fe_2O_3–Zn–K–Cu precursors in H_2

Figure 3 shows the rates of removal of lattice oxygen atoms from Fe_2O_3–Zn–K–Cu precursors using H_2 as the reductant. The amount of oxygen removed was estimated from these data using the reduction of stoichiometric CuO as a calibration standard. The amounts of oxygen for the two peaks in figure 3 show that the reduction of Fe_2O_3 occurs in two steps; Fe_3O_4 first formed and then reduced to form Fe metal. The presence of Cu in Fe–Zn oxides (Zn/Fe = 0.1) causes the Fe_2O_3 reduction to Fe_3O_4 to occur at ∼140 K lower temperature than in Cu-free samples (figure 3(b)); these reduction processes occur at temperatures identical to those required for the reduction of CuO to Cu metal (figure 3(a)). As CuO reduces, Cu crystallites nucleate and provide H_2 dissociation sites, which in turn lead to reactive hydrogen species capable of reducing Fe oxides at relatively low temperatures.

Potassium, shown to be present as K_2CO_3 by X-ray absorption spectroscopy [22], does not influence the reduction of Fe_2O_3, but it weakly inhibits the reduction of Fe_3O_4 to metal Fe. When both Cu and K are present, the reduction profile resembles that for Fe_2O_3–Zn–Cu; Fe_2O_3 reduces at temperatures similar to those required for CuO reduction (∼470 K), except for a small fraction of the Fe_2O_3, which is unaffected by the presence of Cu, apparently because of inefficient contact between some of the Fe_2O_3 and the CuO promoter. The presence of Cu or K does not strongly influence the reduction of Fe_3O_4 to Fe, because thermodynamics

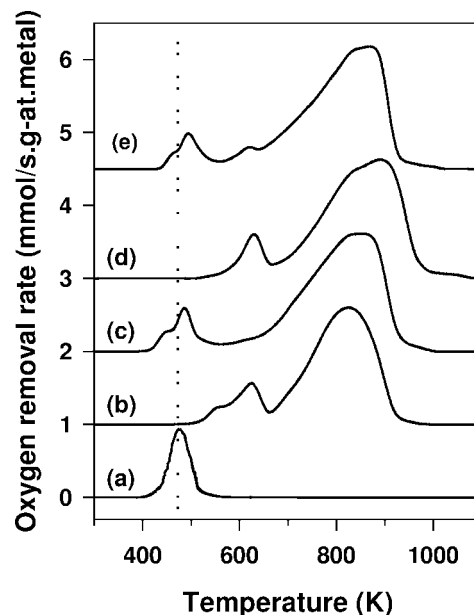and the nucleation of a new crystal structure, and not H_2 dissociation steps, control the reduction rates at these higher temperatures [23,24]. The effects of Cu on the kinetics of removal of lattice oxygen from Fe–Zn oxides suggest that Cu increases the initial rate of nucleation of reduced Fe oxide phases. Consequently, a larger number of nuclei can become available for the crystallization of reduced FeO_x and FeC_x crystallites; higher FTS rates would then be expected when the activation of Fe–Zn oxide precursors occurs in the presence of these promoters.

3.5. Reduction and carburization kinetics of Fe_2O_3–Zn–K–Cu in CO

The individual rates of oxygen removal and of carbon introduction using CO were measured as a function of temperature for Fe_2O_3–Zn–K–Cu oxides by monitoring the concentrations of CO and CO_2 in the effluent stream. Two general stoichiometric reactions are involved in the carburization of Fe oxides. The removal of lattice oxygen occurs *via*

$$Fe_xO + CO \rightleftharpoons Fe_x + CO_2$$
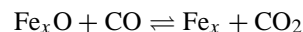
Initially Fe oxides reduce to form CO_2 and a Fe center with valence lower than in Fe_2O_3. In a sequential or alternate step, CO carburizes Fe oxides to form CO_2 and Fe carbides:

$$Fe_xO + 2CO \rightleftharpoons Fe_xC + CO_2$$
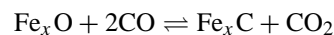
In this step, oxygen removal and carbon deposition occur concurrently. The excess amount of CO consumed relative to the CO_2 produced provides a measure of the amount of carbon that has been retained by the sample. The different CO and CO_2 stoichiometries associated with these two steps,
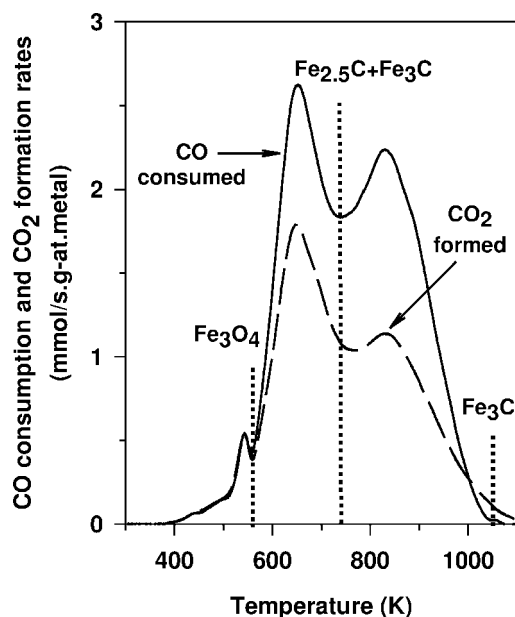
Figure 4. Rates of CO consumption (—) and CO_2 formation (- - -) for the Fe_2O_3–Zn–K_2–Cu_1 sample (Zn/Fe = 0.1) during the reduction and carburization in CO (0.2 g sample, 0.167 K/s ramping rate, 20% CO/Ar, 0.268 mol/h flow rate). (· · ·) Temperatures at which reactions were terminated for XRD measurements (figure 5).
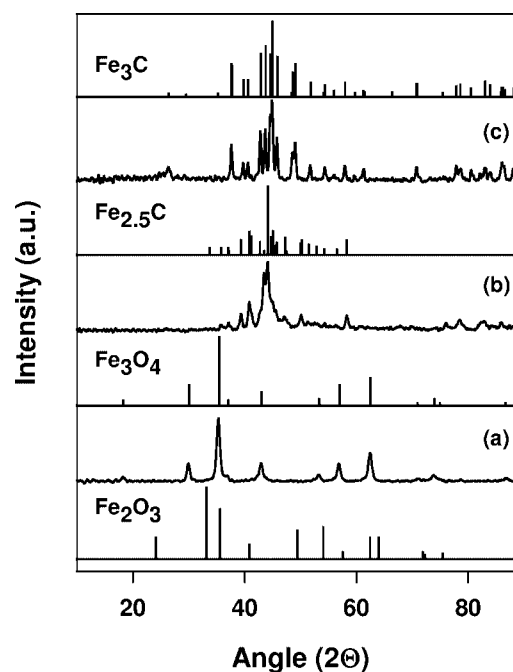

Figure 5. X-ray diffraction patterns showing the phase evolution of the Fe_2O_3–Zn–K_2–Cu_1 oxide (Zn/Fe = 0.1) during the reduction and carburization in CO at (a) 560 K, (b) 730 K, and (c) >730 K (0.2 g sample, 0.167 K/s ramping rate, 20% CO/Ar, 0.268 mol/h flow rate).

allows the net rates of oxygen removal and of carbon deposition steps to be decoupled using the following equations:

$$R_O = \text{oxygen removal rate} = 2R_{CO_2} - R_{CO}, \quad (1)$$

$$R_C = \text{carbon introduction rate} = R_{CO} - R_{CO_2}, \quad (2)$$

where R_{CO_2} is the rate of CO_2 formation and R_{CO} is the rate of CO consumption. We note that this approach remains rigorous even if the actual reactions do not proceed as written, because equations (1) and (2) merely reflect oxygen and carbon mole balances, respectively. Together with the structures detected by X-ray diffraction at various intermediate points in reactions with CO, this approach probes the temperatures required, the rates of reduction and carburization, and the structure and the average stoichiometry of the carbides formed.

CO consumption and CO_2 formation rates are shown in figure 4 for Fe_2O_3–Zn–K–Cu samples as a function of temperature. The stoichiometries for oxygen removal and carbon introduction measured from the areas under these peaks indicate that the reduction/carburization of Fe oxides proceeds in two sequential steps. Fe_2O_3 first reduces to Fe_3O_4 at ~543 K; then, Fe_3O_4 concurrently reduces and carburizes to a mixture of $Fe_{2.5}C$ and Fe_3C in the 543–723 K temperature range. Above 723 K, CO disproportionation occurs *via* the Boudouard reaction, with the formation of excess amorphous carbon; this amorphous carbon is not present in carbide structures formed *via* reactions of CO below 723 K. X-ray diffraction measurements (figure 5) confirmed the sequential nature of the evolution of structure from Fe_2O_3 to Fe_3O_4 and then to mixtures of $Fe_{2.5}C$ and Fe_3C.

Figure 6 shows oxygen removal and carbon introduction rates as a function of temperature for Fe_2O_3–Zn–K–Cu sam-
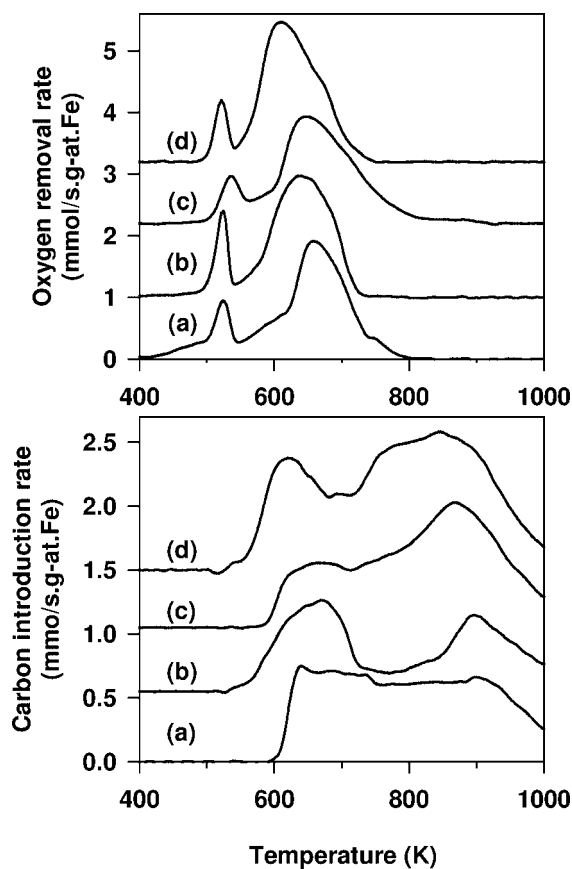
Figure 6. Oxygen removal and carbon introduction rates for the Fe_2O_3–Zn–K–Cu (Zn/Fe = 0.1) samples in CO: (a) Fe_2O_3–Zn, (b) Fe_2O_3–Zn–Cu_1, (c) Fe_2O_3–Zn–K_2, (d) Fe_2O_3–Zn–K_2–Cu_1 (0.2 g sample, 0.167 K/s ramping rate, 20% CO/Ar, 0.268 mol/h flow rate).

ples using CO as the reactant. The areas under the oxygen removal peaks for Fe_2O_3–Zn confirm that Fe_2O_3 is first converted to Fe_3O_4 without any detectable carburization. The temperatures required and the areas under the carbon introduction peaks show that reduced Fe_3O_4 species are then concurrently reduced and carburized to form FeC_x (figure 6(a)). The addition of K and/or Cu to Fe_2O_3 did not influence this reduction–carburization sequence, but the reaction rates increased and the required temperatures decreased when these promoters were present (figure 6 (b)–(d)). Cu increased oxygen removal rates and decreased the temperature required for the reduction and concurrent carburization of Fe_3O_4 by ∼50 K. This effect of Cu on reduction rates was weaker than that observed when H_2 was used as the reductant, apparently as a result of the slower activation of CO relative to H_2 on Cu metal surfaces. The addition of K to Fe_2O_3 led to a shift in the oxygen removal peak to higher temperatures (figure (6c)); the rate of incipient carburization, indicated by the low-temperature shoulder in the carbon introduction peak, was slightly lower than on the unpromoted Fe oxide (figure 6(a)). This may reflect a catalytic effect of K-promoted Fe oxides on CO activation rates [25] or just the faster nucleation of FeC_x crystallites on oxide surfaces promoted with K carbonate. When both K and Cu were present, the combined promoting effects of Cu on oxygen removal steps and of K on CO activation steps led to the highest rates of reduction and carburization of Fe oxide precursors (figure 6(d)).

In summary, K and Cu increased the rates of reduction and carburization of Fe–Zn oxide precursors, and of nucleation of reduced Fe-containing phases (Fe_3O_4 or FeC_x) when CO is used as the reactant. These faster nucleation rates reflect a larger number of nuclei, which ultimately lead to smaller crystallites and to higher active surface areas [17,19]. These promotional effects of K and Cu appear to be mostly textural in nature, a conclusion confirmed by the FTS catalytic data shown in section 3.6.

3.6. Effects of K and Cu on Fischer–Tropsch synthesis rate and selectivity

The promotional effects of Cu and K on the behavior of Fe–Zn FTS catalysts were examined using a tubular reactor with plug-flow hydrodynamics. Fe_2O_3–ZnO catalysts (Zn/Fe = 0.1) with varying K (K/Fe = 0, 0.02 and 0.04) and Cu (Cu/Fe = 0, 0.01, 0.02) contents were used to convert H_2/CO mixtures at 493 K and 3.16 MPa. FTS rates and selectivities are shown in table 2. CO conversion rates increased with K (K/Fe = 0.02) or Cu (Cu/Fe = 0.01) addition, suggesting that the promotion of carburization and reduction rates by these species leads to either a larger number of active sites or to sites with a higher intrinsic activity. These rates were higher on the sample containing both K and Cu as promoters (Fe_2O_3–Zn–K_2–Cu_1) than on Cu-promoted (Fe_2O_3–Zn–Cu_1), K-promoted (Fe_2O_3–Zn–K_2), or unpromoted (Fe_2O_3–Zn) catalysts. The effects of K and Cu on the doubly promoted sample are nearly additive, suggesting an

Table 2
Steady-state performance of Fe_2O_3–Zn catalysts (Zn/Fe = 0.1) with different loadings of K and Cu (H_2/CO = 2, 493 K, 3.16 MPa, CO conversion 14–18%).

K/Fe atomic ratio (×100)	0	0	2	2	2	4
Cu/Fe atomic ratio (×100)	0	1	0	1	2	1
CO conversion rate (mol-CO/h g-at.-Fe)	0.70	0.87	1.23	2.40	2.43	2.49
CO_2 formation rate (mol-CO/h g-at.-Fe)	0.02	0.06	0.10	0.30	0.32	0.30
Hydrocarbon formation rate (mol-CO/h g-at.-Fe)	0.68	0.81	1.13	2.10	2.11	2.19
CO_2 selectivity (%)	2.3	6.5	8.5	12.3	12.9	12.1
CH_4 selectivity (%)[a]	4.8	10.2	1.8	1.8	2.0	2.5
C_{5+} selectivity (%)[a]	81.9	62.1	87.5	87.6	86.7	85.2
1-C_5H_{10}/n-C_5H_{12} ratio	1.9	1.7	1.8	1.8	1.8	2.0
1-$C_{10}H_{20}$/n-$C_{10}H_{22}$ ratio	0.4	0.4	1.7	1.8	1.7	1.7

[a] CH_4 and C_{5+} selectivities are reported on a CO_2-free basis.

almost independent effect of each promoter. The previously reported decrease in FTS rates with increasing K content on Fe–Si oxide precursors was not observed in catalysts made from Fe–Zn precursors [16], possibly because of the higher surface of the precursors or the more dispersed nature of the promoter in the latter samples. For Fe–Zn oxide precursors, no detectable changes in FTS rates or selectivities were observed upon increasing the atomic K/Fe ratio above 0.02 (table 2). Similarly, an increase in Cu/Fe atomic ratios from 0.01 to 0.02 did not influence reaction rates or product selectivities (table 2). Thus, a Cu/Fe ratio of 0.01 and a K/Fe ratio of 0.02 lead to optimum FTS catalytic properties. It appears that the surface density of promoters or the extent to which they contact the Fe oxide precursors does not continue to increase as the Cu or K contents increase above a threshold value. This threshold value is most rigorously expressed as a promoter surface density and it corresponds to ∼1 Cu/nm^2 and ∼2 K/nm^2 [17].

Hydrocarbon formation rates (in mol-CO/h g-at.-Fe) are shown in figure 7 for the various promoted Fe_2O_3–ZnO catalysts as a function of CO conversion. The effects of increasing CO conversion were similar on all catalysts, suggesting that these catalysts show similar kinetic dependences on reactant and product concentrations. CO_2 selectivities are shown as a function of CO conversion in figure 8 and compared at a similar CO conversion value (14–18%) in table 2. CO_2 selectivities increased with increasing CO conversion on all four catalysts (figure 8); they were higher on Fe_2O_3–ZnO promoted by both Cu and K than on unpromoted or singly promoted samples at all conversion levels. H_2O, which forms as a primary product during FTS reactions on Fe catalysts, reacts with CO to give CO_2 via secondary water–gas shift reactions.

The local slope of the curves in figure 8 reflects the contributions from secondary reactions (predominately water–gas shift), while CO_2 selectivities extrapolated to zero conversion reflect the relative rates at which chemisorbed oxygen, formed in CO activation steps, is removed by adsorbed CO (as CO_2) or by adsorbed hydrogen (as H_2O). The slopes
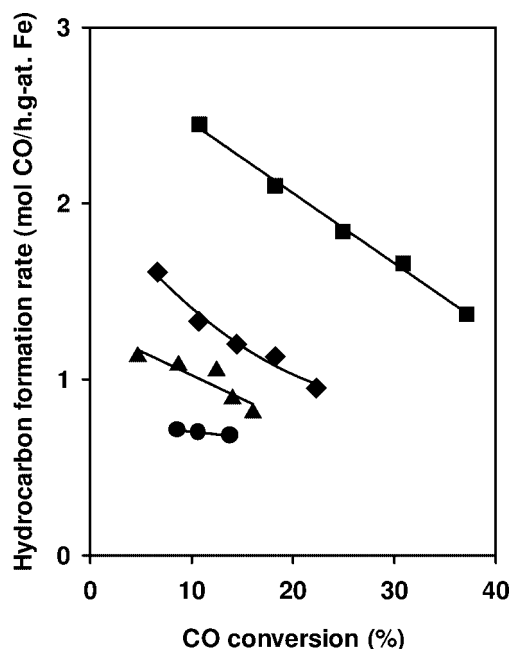
Figure 7. Hydrocarbon formation rates on Fe_2O_3–Zn (●), Fe_2O_3–Zn–Cu_1 (▲), Fe_2O_3–Zn–K_2 (♦), and Fe_2O_3–Zn–K_2–Cu_1 (■) catalysts (493 K, 3.16 MPa, $H_2/CO = 2$).
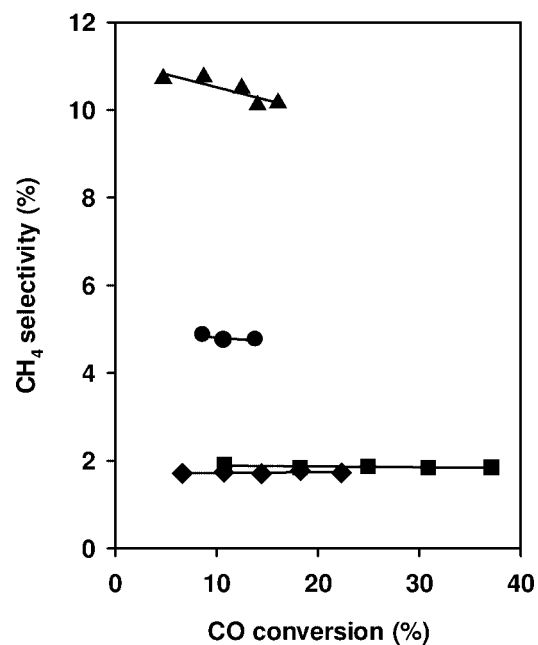
Figure 9. CH_4 selectivities on Fe_2O_3–Zn (●), Fe_2O_3–Zn–Cu_1 (▲), Fe_2O_3–Zn–K_2 (♦), and Fe_2O_3–Zn–K_2–Cu_1 (■) catalysts (493 K, 3.16 MPa, $H_2/CO = 2$).

Figure 8. CO_2 selectivities on Fe_2O_3–Zn (●), Fe_2O_3–Zn–Cu_1 (▲), Fe_2O_3–Zn–K_2 (♦), and Fe_2O_3–Zn–K_2–Cu_1 (■) catalysts (493 K, 3.16 MPa, $H_2/CO = 2$).

presence of Cu predominately influences the intrinsic oxygen removal selectivity by promoting the removal of oxygen using CO. On the other hand, Fe_2O_3–Zn–K_2 and Fe_2O_3–Zn–K_2–Cu_1 showed significantly larger slopes than K-free samples, indicating that the presence of K increases secondary water–gas shift rates, as also reported for Fe–Si oxide precursors [16], without influencing the primary oxygen removal selectivity.

The presence of K in Fe_2O_3–Zn catalysts led to lower CH_4 selectivities (table 2, figure 9) and higher C_{5+} selectivities (table 2, figure 10), apparently by decreasing the availability of H* atoms required for termination of growing chains *via* hydrogen addition reactions to form paraffins. In contrast, the addition of Cu to Fe_2O_3–Zn increased CH_4 selectivities and decreased C_{5+} selectivities (table 2, figure 10). When Cu and K are both present, the tendency of Cu to decrease product molecular weight almost disappears. Potassium also inhibits secondary reactions of α-olefins, such as isomerization to internal or branched olefins and hydrogenation to n-paraffins, by titrating acid sites or uncarbided sites on Fe_2O_3–Zn. The titration of these sites and the apparent decrease in the availability of adsorbed hydrogen also lead to lower rates of secondary hydrogenation reactions. 1-pentene/n-pentane ratios are shown in figure 11 on various catalysts, and also compared in table 2 at similar CO conversions. The olefin content in the K-promoted catalysts increased slightly with CO conversion. This is likely to reflect an inhibiting effect of H_2O or CO_2 on the termination of growing chains by hydrogen addition, as reported previously [14]. The intrinsic olefin/paraffin ratios (extrapolated to zero CO conversion) are actually higher on catalysts without K, but the tendency of K-free catalysts to hydrogenate olefins leads to a marked decrease in olefin content with in-
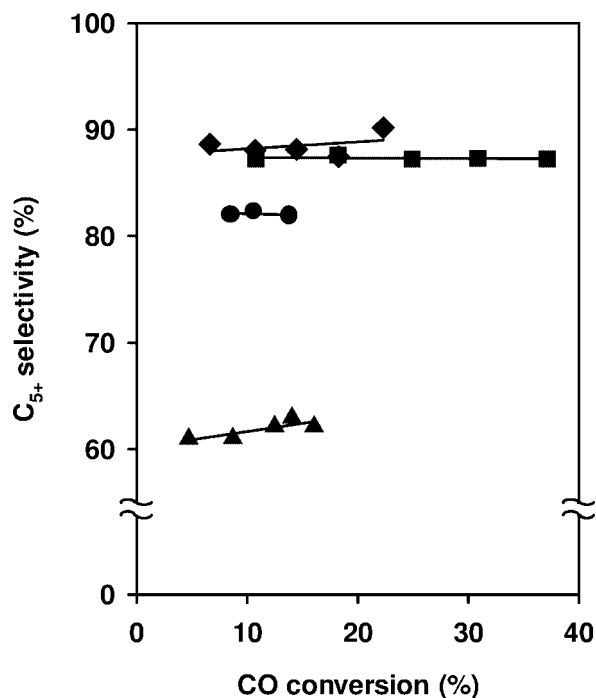
of the CO_2 selectivity curves in figure 8 are similar for the K-promoted Fe_2O_3–Zn–Cu_1 and Fe_2O_3–Zn catalysts, consistent with similar secondary water–gas shift rates. Fe_2O_3-Zn and Fe_2O_3–Zn–Cu_1 catalysts without K resemble each other in their secondary water–gas shift rates, which are lower than those measured on K-containing samples. The lack of effect of Cu is unexpected, in view of the high water–gas shift rates reported on Cu-based catalysts [26]. The

Figure 10. C_{5+} selectivities on Fe_2O_3–Zn (●), Fe_2O_3–Zn–Cu_1 (▲), Fe_2O_3–Zn–K_2 (◆), and Fe_2O_3–Zn–K_2–Cu_1 (■) catalysts (493 K, 3.16 MPa, $H_2/CO = 2$).

Figure 12. 1-$C_{10}H_{20}/n$-$C_{10}H_{22}$ ratios on Fe_2O_3–Zn (●), Fe_2O_3–Zn–Cu_1 (▲), Fe_2O_3–Zn–K_2 (◆), and Fe_2O_3–Zn–K_2–Cu_1 (■) catalysts (493 K, 3.16 MPa, $H_2/CO = 2$).
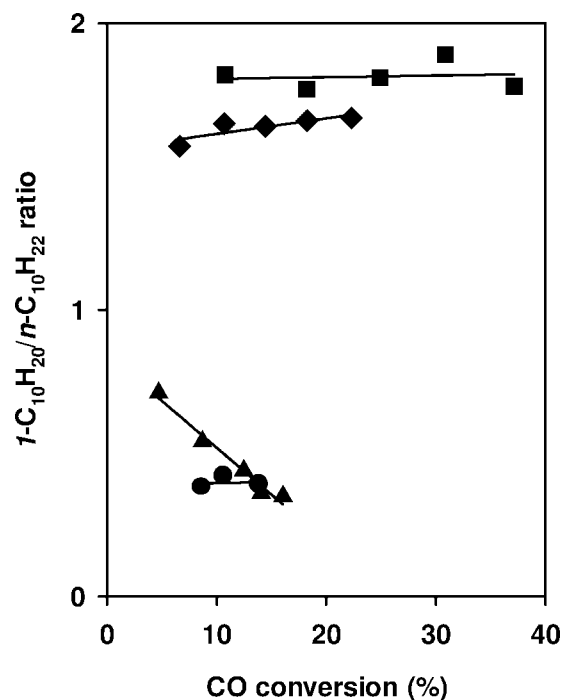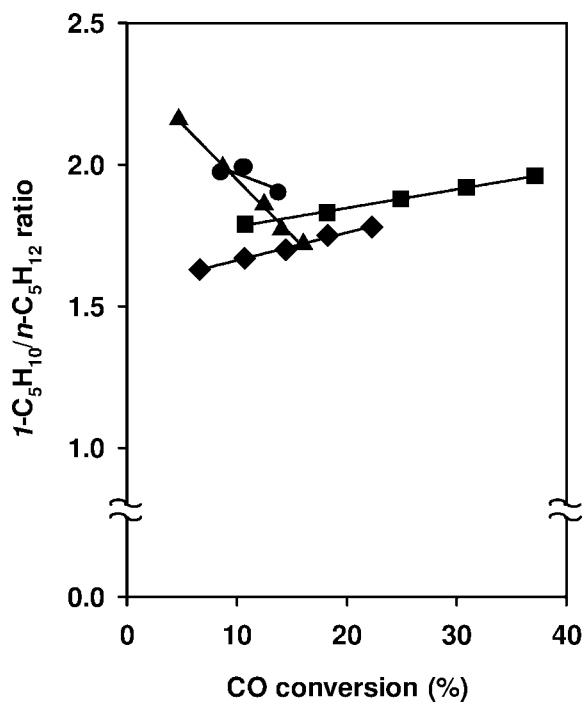
4. Conclusions

Reduction–carburization studies showed that Fe_2O_3 sequentially reduces to Fe_3O_4 and then to a mixture of $Fe_{2.5}C$ and Fe_3C during activation in CO at 540–720 K. Precipitated Fe–Zn oxides form a mixture of Fe_2O_3 and $ZnFe_2O_4$. The latter inhibits sintering of Fe oxide phases at low Zn contents and provides a matrix for isolation of Fe_2O_3 at higher Zn contents, leading to an increase in surface area after thermal treatment and after activation in synthesis gas. Zn also reacts with Fe oxide precursors to form $ZnFe_2O_4$, a phase that does not reduce or carburize during FTS reactions. As a result, intermediate Zn/Fe ratios lead to optimum FTS rates, without any detectable changes in chain growth selectivity. Cu and K do not influence the surface area of Fe oxide precursors. Cu increases the rate of Fe_2O_3 reduction to Fe_3O_4 in H_2, while K promotes the activation of CO and the rate of carburization of Fe_3O_4. During activation in synthesis gas, the combined presence of K and Cu provides routes for the easier formation of Fe_3O_4 using H_2 and its faster carburization using CO. Cu and K both lead to faster nucleation of oxygen-deficient Fe oxides and to the ultimate formation of smaller carbide crystallites with a higher active surface area. As a result, both Cu and K increase FTS rates on catalysts formed by activation in synthesis gas from Fe–Zn oxide precursors. Cu introduces some sites with low chain growth probability and high olefin hydrogenation activity, but such sites are titrated by K. K and Cu also influence the mode of oxygen removal and the rate of secondary water–gas shift reactions. K increases water–gas shift reaction rates, but not the the relative rates at which chemisorbed oxygen is removed by CO or H_2

Figure 11. 1-C_5H_{10}/n-C_5H_{12} ratios on Fe_2O_3–Zn (●), Fe_2O_3–Zn–Cu_1 (▲), Fe_2O_3–Zn–K_2 (◆), and Fe_2O_3–Zn–K_2–Cu_1 (■) catalysts (493 K, 3.16 MPa, $H_2/CO = 2$).

creasing residence time. Similarly, 1-decene/n-decane ratios (figure 12, table 2) are significantly higher in the presence of K and the effects of K are much stronger for the larger olefins, because of their greater propensity for secondary reactions.

after CO activation steps. Cu increases the effectiveness of CO in these primary oxygen removal pathways, but does not influence water–gas shift rates. K increases the olefin content and the average molecular weight of FTS products; and also titrates acid sites and inhibits H_2 dissociation.

Acknowledgement

References

[1] F. Fischer and H. Tropsch, Brennstoff-Chem. 7 (1926) 97.

[2] R.B. Anderson, in: *Catalysis*, Vol. 4, ed. P.H. Emmett (Van Nostrand-Reinhold, New York, 1956) p. 29.

[3] H.H. Storch, N. Golumbic and R.B. Anderson, *The Fischer–Tropsch and Related Syntheses* (Wiley, New York, 1951);
R.B. Anderson, *The Fischer–Tropsch Synthesis* (Wiley, New York, 1984).

[4] M.E. Dry, *The Fischer–Tropsch Synthesis*, Catal. Sci. Technol., Vol. 1, eds. J.R. Anderson and M. Boudart (Springer, New York, 1981) p. 160.

[5] H. Kolbel and M. Ralek, Catal. Rev. Sci. Eng. 21 (1980) 225.

[6] J.W. Niemantsverdriet and A.M. van der Kraan, J. Catal. 72 (1981) 385.

[7] J.A. Amelse, J.B. Butt and L.J. Schwartz, J. Phys. Chem. 82 (1978) 558.

[8] G.B. Raupp and W.N. Delgass, J. Catal. 58 (1979) 348.

[9] R. Dictor and A.T. Bell, J. Catal. 97 (1986) 121.

[10] J.P. Reymond, P. Meriaudeau and S.J. Teichner, J. Catal. 75 (1982) 39.

[11] S. Kuivila, P.C. Stair and J.B. Butt, J. Catal. 118 (1989) 299.

[12] S. Huang, L. Xu and B.H. Davis, Fuel Sci. Techol. Int. 11 (1993) 639.

[13] E. Iglesia, S.C. Reyes, R.J. Madon and S.L. Soled, Adv. Catal. 39 (1993) 221.

[14] S. Soled, E. Iglesia, S. Miseo, B.A. DeRites and R.A. Fiato, Topics Catal. 2 (1995) 193.

[15] S. Soled, E. Iglesia and R.A. Fiato, Catal. Lett. 7 (1990) 271.

[16] A.P. Raje, R.J. O'Brien and B.H. Davis, J. Catal. 180 (1998) 36.

[17] S. Li, S. Krishnamoorthy, A. Li, G.D. Meitzner and E. Iglesia, J. Catal., submitted.

[18] R.J. O'Brien, L. Xu, R.L. Spicer, S. Bao, D.R. Milburn and B.H. Davis, Catal. Today 36 (1997) 325.

[19] S. Li, G.D. Meitzner and E. Iglesia, J. Phys. Chem. B, in press.

[20] S. Li, G.D. Meitzner and E. Iglesia, J. Phys. Chem. B, submitted.

[21] D.R. Lide and H.P.R. Frederikse, eds.; *Handbook of Chemistry and Physics*, 75th Ed. (The Chemical Rubber Company Press, Boca Raton, 1994).

[22] S. Li, G.D. Meitzner and E. Iglesia, unpublished results.

[23] M.J. Tiernan, P.A. Barnes and G.M.B. Parkes, J. Phys. Chem. B 105 (2001) 220.

[24] H.H. Kung, *Transitional Metal Oxides*, Stud. Surf. Sci. Catal. 49 (1989).

[25] G.A. Somorjai, Catal. Rev. Sci. Eng. 23 (1981) 189.

[26] R. Habermehl and K. Atwood, Am. Chem. Soc. Div. Fuel. Chem. Prepr. 8 (1964) 10.